Proceedings of the 2007 American Control Conference
Marriott Marquis Hotel at Times Square
New York City, USA, July 11-13, 2007

Experiments of trajectory generation and obstacle avoidance for a UGV

David Vissière, Dong Eui Chang, and Nicolas Petit

***Abstract*— In this paper, we report results of investigations conducted on a mobile robotic experiment developed at the DGA Laboratoire de Recherche en Balistique et Aérodynamique in a joint work with École des Mines. The vehicles under consideration are in fact similar to unicycles. We investigate a flatness based approach (combining open-loop optimization and closed loop tracking) and gyroscopic forces control laws. Experimental results are exposed. A theoretical proof of obstacle avoidance for a gyroscopic scheme is presented.**

INTRODUCTION

The context of our study is the *network centric warfare* (as defined in [9]) program "Bulle Opérationnelle Aéroterrestre" (BOA), led by the Délégation Générale pour l'Armement (DGA) for the French Department of Defense. It is a vast project in which ground, airborne and marine units are asked to cooperate in order to fulfill a wide range of possible missions. In particular, autonomous vehicles are asked to bring fire power, communications, intelligence. Among others, several mission goals are out-of-sight shooting, robust telecommunication, target laser designation in dangerous areas, data-link, and hardware supply. A typical behavior of such cooperation in the BOA environment is depicted in Figure 1. For this project, it was decided to construct several prototypes to stress the needs in missions of military interest. Interestingly, automatic control appears as one of the key challenges. In practical operations, there is definitely a need for real-time control laws for guidance of autonomous vehicle. In facts, it is desired to alleviate the human operators burden. The more autonomous the vehicles are, the better. Two problems are identified: satisfy the mission goals and deal with field uncertainty. Among these uncertainties are obstacles that can not be accounted for at the mission preparation level (these obstacles may have appeared since, or may be invisible or hidden to surveillance devices). There can also be physical disturbances such as wind gusts, and unknown ground to wheels contacts to name a few. In this context, we are designing a twofold experimental setup. The first part we present here is a ground platoon. So far, we have focused on a single vehicle (UGV). Coordination issues are out of the scope of our current investigations. The second half is a team of small-sized helicopters. They will be presented in a forthcoming publication. In this paper, we focus on a simple military type scenario. Its consists of reaching a single target, possibly by following a prescribed path. One or several obstacles can be encountered. They are unknown but their size is upper bounded. The control laws that we propose have to deal with the vehicles input constraints, mission objectives, and have no information from outside once the mission is started. Onboard sensors are the sole information available to avoid unknown obstacles. In this paper we focus on two different control techniques, that we would like to combine in the future. The first one is an off-line optimal trajectory generation technique complemented by a real-time closed loop controller. The second one is a local obstacle avoidance technique using gyroscopic forces as presented in [2]. Combining the two approaches could be done in the following way. Before an obstacle is met, the vehicles should track in closed loop (using on board sensors) the optimal trajectory computed during the mission preparation phase. When an obstacle is detected, the control should switch to the obstacle avoidance phase, slowing down and passing by the obstacle. Once a point on the initial trajectory is approximatively reached, the controller should switch back to the first control phase. Certainly, designing appropriate switching strategies is not an easy task and will require further investigations.

Fig. 1. A typical coordinated airborne and ground platoon as envisionned in the BOA projet. ©BD MEDIAS for Délégation Générale pour l'Armement (DGA).

The paper is organized as follows. In section I, we briefly describe the ground vehicle, its dynamics and onboard systems (including CPU and sensors). The vehicle under consideration (a Pioneer IV from MobileRobots$^{\mathrm{TM}}$) has the

D. Vissière (corresponding author) is "Ingénieur de l'Armement" in the Délégation Générale pour l'Armement (DGA) of the French Department of Defense. He is also a PhD candidate in Mathematics and Control, Centre Automatique et Systèmes, École des Mines de Paris, 60, bd St Michel, 75272 Paris, France david.vissiere@dga.defense.gouv.fr

D. E. Chang is Assistant Professor in the Department of Applied Mathematics, University of Waterloo Waterloo Ontario, N2L 3G1 CANADA

N. Petit is with the Centre Automatique et Systèmes, École des Mines de Paris, 60, bd St Michel, 75272 Paris, France

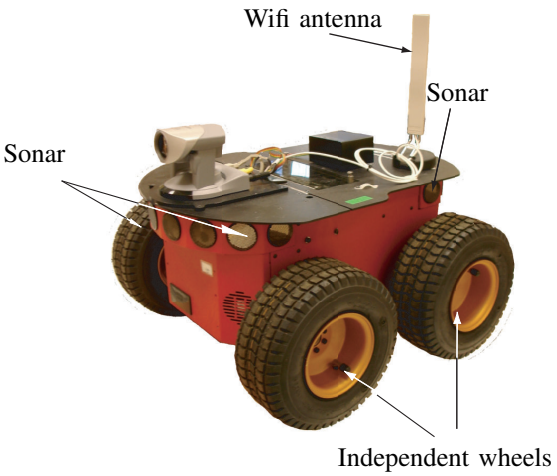

Fig. 2. Pioneer IV vehicle (side view and front view). Four independent wheels, with 16 sonars, one axis gyroscope, odometers, wireless datalink, and onboard CPU.

same dynamics as the unicycle. In section II, we use its flatness property to parameterize and optimize its trajectories. Constrained minimum time problems are considered. Then, we use a dynamic linearizing feedback for tracking purposes. Experimental results are presented. In section III, we consider gyroscopic forces controllers. Using second order schemes (from the literature [2]), we detail experimental results. A known problem is the possibility of zero velocity collision (early pointed out in [2]). For that reason, we propose a first order controller and actually prove a new result concerning convergence under assumptions on the size of the obstacle. This constructive proof can serve as a guideline for tuning.

I. Vehicles under consideration

A. Vehicles description

Our experimental testbed includes three MobileRobots$^{\text{TM}}$ Pioneer 3-AT vehicles similar to the one depicted in Figure 2. These vehicles have 4 electrically powered independent wheels and are capable of running outdoor. The onboard system consists of a Pentium III 800MHz based PC104 system running under Linux, 16 sonars (8 forward and 8 rear) located on the sides of the main frame (above the wheels), a one-axis gyroscope, and a wireless network adapter. It is possible to derive localization information from odometers. Each vehicle is equipped with in-wheels 100 tick encoders with inertial correction to compensate for skid steering. By default, the vehicle does not possess any GPS. We decided to install a uBlox$^{\text{TM}}$ TIM-LR with added antenna. As will be detailed next, we designed our own filter for GPS/odometer/gyroscope hybridation.

B. Vehicle dynamics

Assuming wheels on the same side of the vehicle have the same velocity (i.e. the vehicle behaves like a tank) it is possible to model the dynamics under the nonholonomic unicycle form studied in [5], [10]

$$\begin{cases} \dot{x} = \dfrac{(v_1+v_2)}{2}\cos\theta, \quad \dot{y} = \dfrac{(v_1+v_2)}{2}\sin\theta, \\ \dot{\theta} = \dfrac{(v_2-v_1)}{2l} \end{cases} \tag{1}$$

where x, and y denote the position of the vehicle, θ denotes its orientation angle, and v_1, and v_2 are the speeds of the left side and right side wheels, respectively. This model can be experimentally validated with fitted coefficient $l = 294$ mm. Indoor maneuvers are consistent with motions calculated through numerical integration of (1). Typical errors are of 10 cm for a 4 m wide curves and straight lines trajectory over 60 s.

II. Trajectory generation and tracking

A. Open loop design

The two inputs system (1) is flat [4], i.e. its trajectories can be summarized by those of two flat outputs x and y. Considering x and y, one can recover the other variables, i.e. the remaining state θ and the two controls, from x, y and their derivatives. Explicitly,

$$\theta = \arctan(\frac{\dot{y}}{\dot{x}}) \tag{2}$$

$$v_1 = \sqrt{\dot{x}^2+\dot{y}^2} - l\frac{\ddot{y}\dot{x}-\dot{y}\ddot{x}}{\sqrt{\dot{x}^2+\dot{y}^2}} \tag{3}$$

$$v_2 = \sqrt{\dot{x}^2+\dot{y}^2} + l\frac{\ddot{y}\dot{x}-\dot{y}\ddot{x}}{\sqrt{\dot{x}^2+\dot{y}^2}} \tag{4}$$

Thanks to this property, constrained trajectory optimization can be performed using the approach proposed in [6]. The flat outputs histories are then parameterized using B-splines functions, and, in considered cost functionals and constraints variables, are substituted with their expressions (2), (3), and (4). Here, we consider two different constrained minimum time problems.

1) Optimal trajectory along a prescribed path: The first problem we consider corresponds to the case of a well described path (e.g. a road) the vehicle has to follow as fast as possible, under its dynamic constraints. Given a path $[0,1] \ni s \mapsto (x^{\text{ref}}(s), y^{\text{ref}}(s)) \in \mathbb{R}^2$, it is desired to determine T and $[0,T] \ni t \mapsto \sigma(t) \in [0,1]$ solution of the following optimal control problem

$$\min_{\sigma,T} T$$

subject to the following contraints (where ϵ is a strictly positive constant)

$$\begin{cases} T > 0, \quad \sigma \in \mathcal{C}^2[0,T], \quad \sigma(0) = 0, \quad \sigma(T) = 1, \\ \forall t \in [0,T], \quad \dot{\sigma}(t) > 0, \\ |v_i(t)| \leq v_{\max} \quad i \in \{1,2\}, \\ |\dot{v}_i(t)| \leq A_{\max} \quad i \in \{1,2\} \end{cases} \tag{5}$$

The last inequality can be omitted because (v_1, v_2) does not need to be differentiable (it is convenient to include this last constraint to obtain smooth control histories). If obstacles locations are known, they can be included as state constraints.

2) Free trajectory planning: In a second setup, we optimize over the possible trajectories originating in a given point A, reaching a desired target point B, and avoiding known obstacles. It is desired to find the solution of the following optimal control problem

$$\min_{x,y,T} T$$

subject to the constraints (where ϵ is a strictly positive constant)

$$\begin{cases} T > 0, \quad (x,y) \in \left(\mathcal{C}^2[0,T]\right)^2, \\ (x(0), y(0))^T = A, \quad (x(T), y(T))^T = B, \\ \forall t \in [0,T], (x(\sigma(t)), y(\sigma(t))) \notin \text{obstacles}, \\ |v_i(t)| \leq v_{\max} \quad i \in \{1,2\}, \\ |\dot{v}_i(t)| \leq A_{\max} \quad i \in \{1,2\}, \\ \dot{x}^2 + \dot{y}^2 \geq \epsilon \end{cases}$$

The last constraint is added to avoid the singularity of our dynamic feedback controller around zero velocity.

3) Numerical treatment: Those two problems can be rewritten using only the parameter T and the flat outputs x and y or σ (in the first problem) by substituting v_1 and v_2 in the constraints by their expressions in terms of first and second derivatives of the flat outputs (3) and (4). In the case of constraints given by (5), v_1 and v_2 are computed through the time derivatives of $t \mapsto x^{ref}(\sigma(t))$ and $t \mapsto y^{ref}(\sigma(t))$. Then, the variables are represented by basis functions (typically B-splines). The induced nonlinear program (NLP) can be solved using standard packages (e.g. NPSOL or SNOPT). Compared to a standard collocation approach, in which every state and control variables is represented by distinct basis functions, the proposed substitution technique yields a reduction in the number of variables. This positively impacts on the computational burden of NLP solving (as noted in [7], [1]). Typically, using B-Splines and the Matlab Optimization toolbox, either problem can be solved with a reasonable accuracy in less than 5 sec on a 1GHz PC (this time increases for complex trajectories where the number of B-splines coefficients can get large). Interestingly, this remark stresses the possibility of real-time trajectory updates as proposed in [8] (for receding horizon control techniques or on-demand mission reconfiguration). Finally, once the optimal transient time T and flat outputs histories (x, y) are found, the open-loop control values are recovered from (3) and (4).

B. Tracking

Although the unicycle model is experimentally quite accurate, as noted in Section I-B, there is definitely a need for closed loop control in our experimental setup. The main unmodelled disturbance is slipping (especially during outdoor maneuvers). The previous open-loop strategy can be complemented by the following closed loop dynamic controller. Considering second derivatives of the flat outputs we get

$$\ddot{x} = \dot{u}_1 \cos\theta - u_1 u_2 \sin\theta, \quad \ddot{y} = \dot{u}_1 \sin\theta + u_1 u_2 \cos\theta$$

where we note $u_1 = \frac{v_1+v_2}{2}$ and $u_2 = \frac{v_1-v_2}{2l}$. There is a globally well-defined change of coordinates between the vector $(\ddot{x}, \ddot{y})^T$ and $(\dot{u}_1, u_1 u_2)^T$, though the θ angle rotation matrix. Imposing stable dynamics of the form

$$\ddot{x} = \ddot{x}^{\text{sp}} - k_1(x - x^{\text{sp}}) - k_2(\dot{x} - \dot{x}^{\text{sp}}) \quad (6)$$

$$\ddot{y} = \ddot{y}^{\text{sp}} - k_1(y - y^{\text{sp}}) - k_2(\dot{y} - \dot{y}^{\text{sp}}) \quad (7)$$

can be achieved through the following dynamic feedback

$$\dot{u}_1 = \cos\theta\ddot{x} + \sin\theta\ddot{y}, \quad u_2 = \frac{1}{u_1}(-\sin\theta\ddot{x} + \cos\theta\ddot{y})$$

where $\ddot{x}$ and $\ddot{y}$ are substituted with the following expressions derived from (6) and (7)

$$\ddot{x} = \ddot{x}^{\text{sp}} - k_1(x - x^{\text{sp}}) - k_2(u_1\cos\theta - \dot{x}^{\text{sp}})$$
$$\ddot{y} = \ddot{y}^{\text{sp}} - k_1(y - y^{\text{sp}}) - k_2(u_1\sin\theta - \dot{y}^{\text{sp}})$$

This dynamic feedback controller has a single singularity at $u_1 = 0$. This corresponds to a loss of controllability when the vehicle speed is zero. This singularity is avoided, in the open-loop design, by the constraints specified in the optimal control problem.

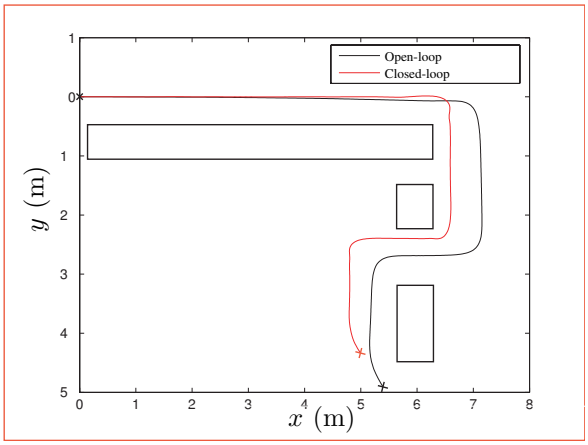

Fig. 3. Indoor closed loop tracking of an optimal trajectory. One can observe the open-loop drift of the vehicle.

C. Indoor results

A complex manoeuver can be accomplished indoor. In Figure 3, the vehicle has to avoid three obstacles, make a turn and eventually reach a prescribed target. Indoor, only odometers and the gyroscope can be used on board to determine the position of the vehicle. As can be seen in Figure 3, the open-loop behavior shows a significant drift, probably due to unaccuracies in the slipping laws during sharp turns (and also to unmodelled dynamics such as wheels inertia, and electric drive current saturations). It is overcome by the

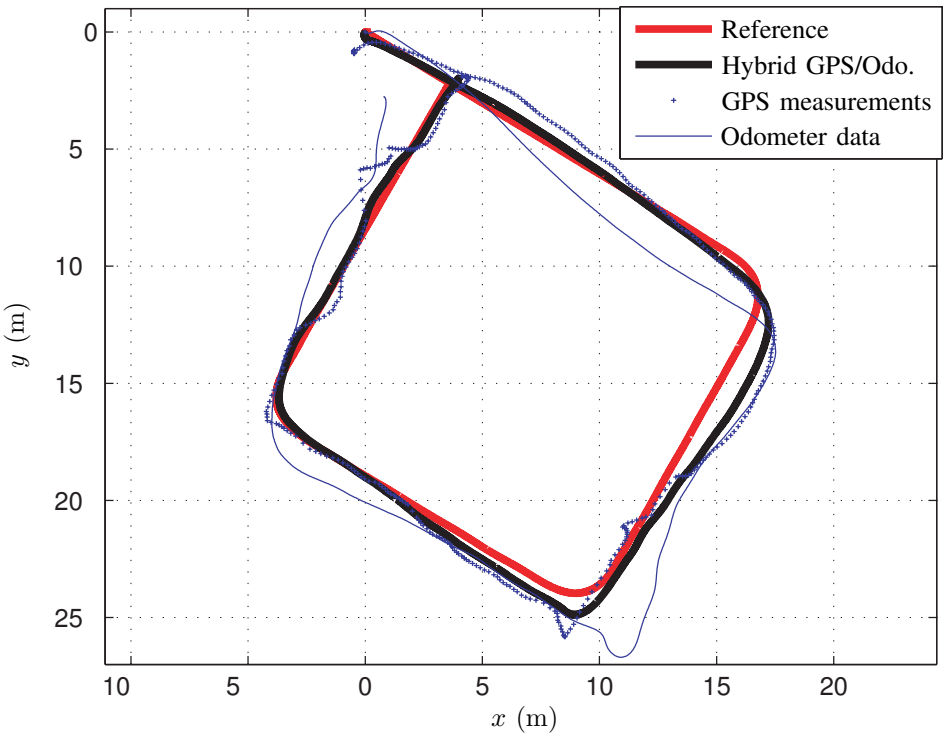

Fig. 4. Spinning around a tree. Y axis is pointing North. X axis is pointing East.

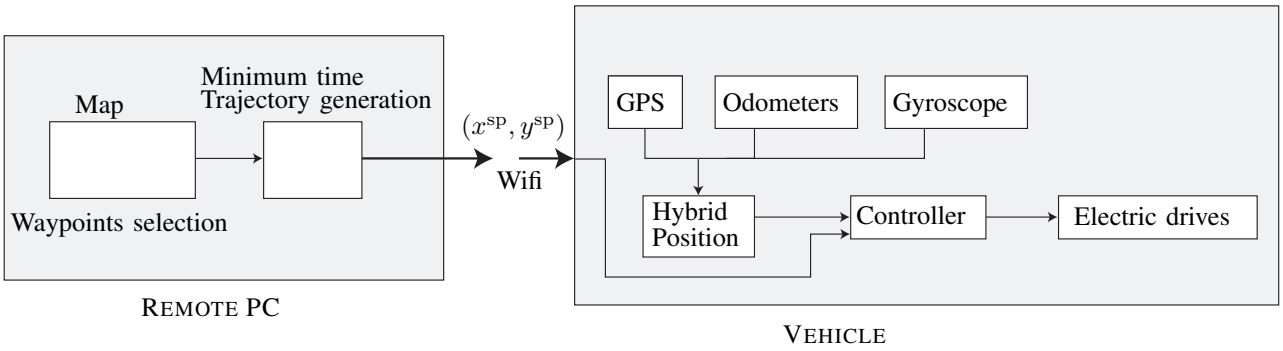

Fig. 5. Human machine interface. Trajectory is designed on a remote PC according to user's requests (waypoints selected on a map) and minimum time transients control objectives. On board the vehicle, GPS sensors and odometers feed a hybrid positioning system used in closed loop to actuate the electric drives.

closed loop feedback presented in Section II-B. However, one should notice that the measurements do not guarantee that the actual position of the vehicle matches the reference trajectory. In facts, the odometers often provide misleading information, especially during large maneuvers. For long term outdoor experiments, they need to be complemented by absolute measurements such as those from a GPS. This issue is addressed in the following section.

D. Outdoor results

The proposed methodology was tested outdoor. The Pioneer vehicle was equipped with an onboard GPS (a uBlox^{TM} TIM-LR). Its signals were fed into an observer along with signals from the odometers and the gyroscope to reconstruct the vehicle position. A Matlab-based human machine interface was designed following the structure presented in Figure 5. On a remote PC, several waypoints are chosen on a map. Automatically, a smoothing procedure defines a reference path that is fed into the optimal trajectory generation software implemented in Matlab. Once the optimal trajectory is found, it is sent to the remote vehicle through the Wifi datalink under the form of a collection of sampled data. Then, the vehicle starts tracking this trajectory. Typical obtained results are depicted in Figure 4 and in Figure 6. In

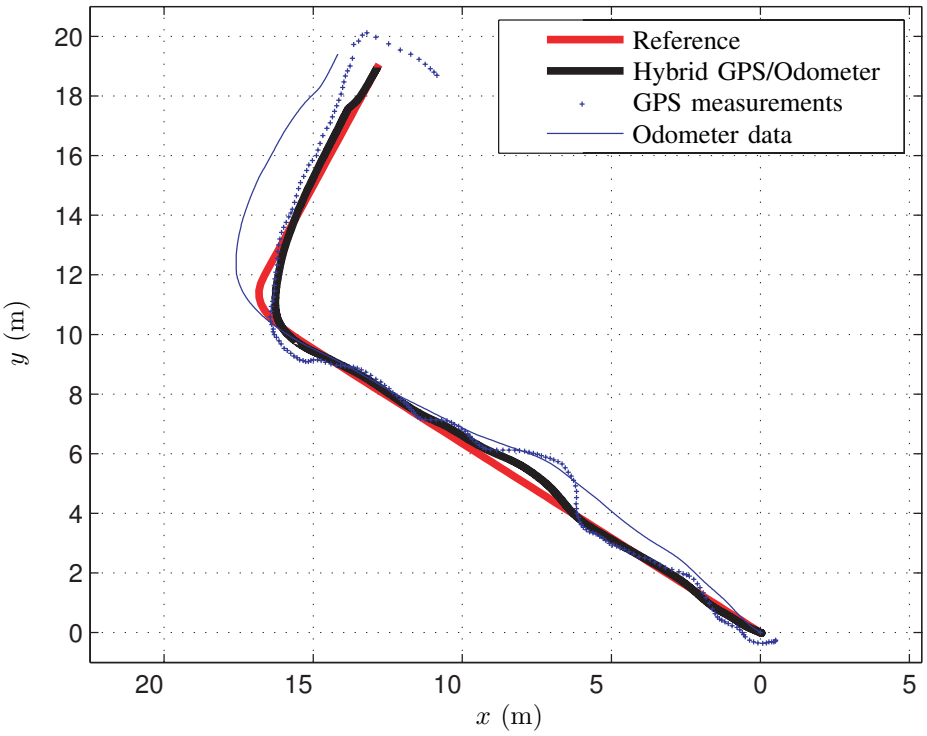

Fig. 6. Turning around a corner. Y axis is pointing North. X axis is pointing East.

these figures, several plots indicate the quality of tracking. Noticeably, neither the GPS nor the odometer can be used as sole positioning system for sake of closed loop control. The GPS suffers from low pass drift, noises, and jumps, while the odometer signal is altered by a long term drift. Both provide misleading information in a closed loop context. Yet, it is possible to reconciliate the data as we did and obtain an estimate that is suitable for tracking the reference trajectory. These observations clearly appear when inspecting results presented in both Figure 4 and 6.

III. Gyroscopic forces

The previously presented open-loop and closed-loop control strategies do not take into account obstacles that are not known in advance. Though it is possible to update the optimal path along the way (e.g. in a receding horizon fashion), once an obstacle is discovered, we prefer to use a control law dedicated to deal with these obstacles found at close range. An ideal candidate is the so-called "gyroscopic forces" law [2], [3]. As will appear next, while being very effective and simple to implement, they do not guarantee collision avoidance. In the following, after recalling the fundamentals of this technique, we propose an alternate formulation (first order) for which we prove convergence and obstacle avoidance.

A. Notations

We consider a vehicle, a target and a single circular obstacle that must be avoided. In the following, we note R the obstacle radius, r the detection radius, A the center of the obstacle, B the most distant point from the origin in the disc $C(A,r)$, $q=(x,y)^T$ the position of the center of gravity of the vehicle, q_T the target point. Further, $dq \triangleq (A-q)\frac{\|A-q\|-R}{\|A-q\|} \in \mathbb{R}^2$ denotes the vector difference between q and its orthogonal projection onto the obstacle, ε is a scalar valued function defined by

$$q \mapsto \varepsilon(q) = \begin{cases} -\ \text{sign det}(q_T - q, dq) \\ \quad \text{if } \|dq\| \leq (r-R) \\ \quad \text{and } |\arg(q-q_T)| \leq \arcsin(R/OA) \\ \\ 0 \quad \text{otherwise} \end{cases}$$

We use $V_{\max}$ a (positive) avoidance constant. Two geometric points play a particular role in the convergence analysis. These are noted T_1, and T_2 (see Figure 8). They are located at the intersections of the circle C(A,R) and the two tangent lines originating in 0. Finally, we note $H = (OA) \cap C(A,R)$.

1) Proposed gyroscopic scheme: The second order scheme usually reported in the literature is given in (8) (where $\wedge$ stands for the logical AND)

$$\ddot{q} = \begin{pmatrix} -2 & -w(q,\dot{q}) \\ w(q,\dot{q}) & -2 \end{pmatrix} \dot{q} - (q - q_T)$$

$$w(q,\dot{q}) = \begin{cases} \dfrac{\pi V_{\max}}{d(q)} \text{ if } \{d(q) \leq r\} \wedge \{d(q).\dot{q} > 0\} \wedge \{\det(d(q),\dot{q}) \geq 0\} \\ -\dfrac{\pi V_{\max}}{d(q)} \text{ if } \{d(q) \leq r\} \wedge \{d(q).\dot{q} > 0\} \wedge \{\det(d(q),\dot{q}) < 0\} \\ 0 \quad \text{otherwise} \end{cases} \tag{8}$$

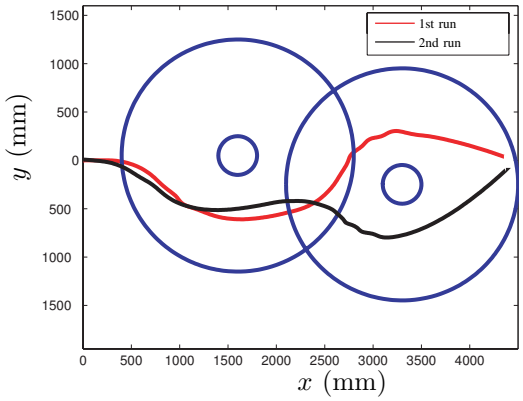

Fig. 7. Indoor experimental results using gyroscopic forces. Circular obstacles are represented with their detection shells. Trajectories can bifurcate due to measurement noises.

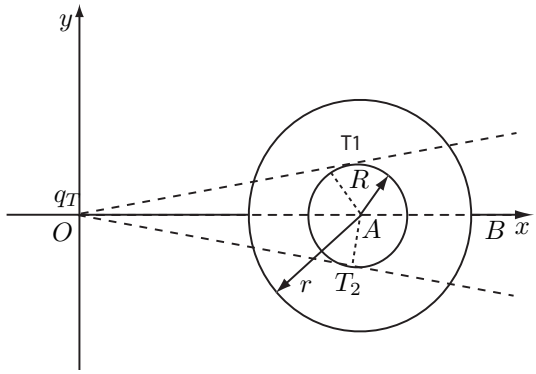

Fig. 8. Notations for gyroscopic forces control law.

with w given in (8). We tried this method in practical experiments with good success. Typical obtained (closed-loop) trajectories are reported in Figure 7. The method appears to be quite sensitive to sensor noises. There can be some bifurcations as observed in this same figure, depending which side of the vehicle the obstacle is first detected on. Simulation results proposed in [2], [3] are also very interesting and show the versatility of the approach. But, there are possibilities of zero velocity collisions (one can refer to [2] for a discussion on this). These are unacceptable in practice because they would result in a complete stop of the vehicle. To address this problem, we propose a first order scheme and actually prove its convergence. It should be soon tested on the experiment.

B. Obstacle avoidance result

Our goal is to prove that under a condition on $V_{\max}$, irrespective of initial conditions, the following differential equation has a unique solution that exponentially converges toward the target without intersecting the obstacle

$$\dot{q} = (q_T - q) + \varepsilon(q) V_{\max} \begin{pmatrix} 0 & -1 \\ 1 & 0 \end{pmatrix} (q_T - q)$$

For sake of analysis, the target is set to 0 and the obstacle center position is set to $(1,0)$. Other configurations can be easily obtained by appropriate homothetic transformation, translation and/or rotation. Under this simplifying assumption, we are left with the following equation

$$\dot{q} = \begin{pmatrix} -1 & \varepsilon(q)V_{\max} \\ -\varepsilon(q)V_{\max} & -1 \end{pmatrix} q \tag{9}$$

The proof is organized as follows. As can be easily seen, the system is globally exponentially stable in the absence of the obstacle. First, we analyse the convergence to zero of (9). This results in Proposition 1. Then, we construct a positively invariant set Δ (see Definition 1) that excludes the obstacle. In a first move, we focus on a particular trajectory that serves as a boundary for Δ. We prove that, under an explicit tuning condition, this trajectory does not intersect with the obstacle in Proposition 2. Finally, we prove in Theorem 1 that Δ is positively invariant by equation (9), and that, eventually, every trajectory starting in Δ converges to the target.

Proposition 1: Every trajectory of (9) asymptotically converges to 0.

Proof: Note $V(q) = \frac{1}{2}\|q\|^2$. It follows that

$$\dot{V}(q) = \langle q, -q - \varepsilon(q) V_{\max} \begin{pmatrix} 0 & -1 \\ 1 & 0 \end{pmatrix} q \rangle = -2V(q)$$

and, then,

$$\|q(t)\| = \|q(0)\| \exp(-t) \tag{10}$$

which proves the result. ■

A more difficult task is to guarantee that trajectories do not collide with the obstacle. We now construct a set being positively invariant by (9). Its boundaries are a particular trajectory on one side, and its symmetric curve on the other side. To prove that it does not contain trajectories intersecting the obstacle, we compute lower bounds on angles of rotation and conclude by contradiction. This constructive proof yields a sufficient lower bound on $V_{\max}$.

a) A particular trajectory $\mathcal{T}$: We consider $\mathcal{T}$ the trajectory originating in B (see Figure 8), i.e. the set of points $q(t)$, $t \in [0, +\infty[$ solution of (9), with $q(0) = B$. Equation (9) can be analytically solved under the form

$$q(t) = (1 + r)\exp(-t)\exp(-\imath(t\varepsilon(q)V_{\max})) \tag{11}$$

This trajectory does not intersect the tangent line (OT_1). It can not cross the bisecting line (OA) either. To do so, the argument of q need to decrease. Yet, in this zone of the plane, the argument is strictly increasing as can be seen in equation (11) with $\varepsilon = 1$. In summary, $\mathcal{T}$ entirely lies in the inner sector $((OT_1),(OA))$. This allows us to introduce the following definition.

Definition 1: We denote by Δ the complementary set of the interior of the closed curve constructed with $\mathcal{T}$ and the curve symmetrical to it with respect to the bisecting line (OA). Δ is a closed subset of $\mathbb{R}^2$.

As we will prove it, Δ is positively invariant by equation (9). Provided that the initial condition is chosen inside Δ, the trajectory avoids the obstacle. To prove this point, we need to show that the obstacle has an empty intersection with Δ.

b) A property of $\mathcal{T}$:

Proposition 2: Trajectory $\mathcal{T}$ does not intersect the obstacle provided the following inequality holds

$$V_{\max} \geq \sqrt{\frac{-1}{2} + \sqrt{\frac{1}{2} + \frac{\pi^2 R^2}{\log^2(\frac{1+r}{1+R})}}} \tag{12}$$

Proof: We proceed by contradiction. Assume that the trajectory intersects the circle C(A,R). Then, there exists a unique first-time intersection $(t_2, q_2) \in \mathbb{R}^+ \setminus 0 \times \mathbb{R}^2$ such that $q_2 = q(t_2)$ solution of (9) is on $C(A,R)$. Also, there exists a unique $(t_1, q_1 = q(t_1)) \in \mathbb{R}^+ \setminus 0 \times \mathbb{R}^2$ defined as follows. Consider $[0,t_2] \ni t \mapsto Q(t) = ||q(t) - A|| \in \mathbb{R}$. This mapping is continuous over the compact set $[0,t_2]$. Thus, the set $Q^{-1}(r) \triangleq \{t \text{ s.t. } Q(t) = r\}$ is compact and non-empty (it contains 0 by construction). Therefore, it has a maximum element t_1. By construction, the set $\{q(t), t \in [t_1,t_2]\}$ lies in between the two circles $C(A,R)$ and $C(A,r)$ (we call this zone the "detection shell"). We now look for a lower bound on $t_2 - t_1$ to compute a lower bound on the time spent inside the detection shell. Over $[t_1,t_2]$, the argument of $q(t)$ is increasing, as implied by (9) with $\varepsilon = -1$. Let us compute a lower bound for $\frac{||q_1||}{||q_2||}$. Consider $[0, \arcsin(R)] \ni \alpha \mapsto z(\alpha) \in \mathbb{R}$ as the module of the point of the circle $C(A,R)$ with α argument and largest module. This point is represented in Figure 9. Simple calculations yields

$$z(\alpha) = \cos(\alpha) + \sqrt{\cos^2(\alpha) + R^2 - 1} \tag{13}$$

Let us define $\tilde{q}_2$ as the intersection of the line $(0q_1)$ with $C(A,R)$. Recalling the mapping $\alpha \mapsto z(\alpha)$ is decreasing, one can derive $\frac{||q_1||}{||q_2||} \geq \frac{||q_1||}{||\tilde{q}_2||}$, since $0 \leq \arg(q_1) = \arg(\tilde{q}_2) \leq \arg(q_2) \leq \arcsin(R/OA)$. Further, after several lines, one can derive

$$\begin{aligned}\frac{||q_1||}{||q_2||} \geq \frac{||q_1||}{||\widetilde{q_2}||} &= \frac{\cos(\alpha) + \sqrt{\cos^2(\alpha) + r^2 - 1}}{\cos(\alpha) + \sqrt{\cos^2(\alpha) + R^2 - 1}} \\ &\geq \frac{1+r}{1+R}\end{aligned}$$

Using equation (10), we get $\frac{e^{-t_1}}{e^{-t_2}} = \frac{||q_1||}{||q_2||} \geq \frac{1+r}{1+R}$. Therefore,

$$t_2 - t_1 \geq \log(\frac{1+r}{1+R}) \tag{14}$$

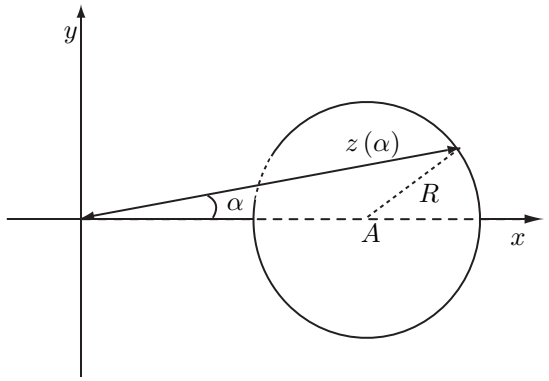

Fig. 9. Notations for the gyroscopic forces control scheme.

Using this lower bound for the time spent in the detection shell, we now look for a lower-bound on the distance $\|q(t) - A\|$ when t varies over $[0,t_2]$. We will prove that this bound is larger than R which contradicts the intersection assumption.

Let us consider $T_{out} = t_1 + \frac{1}{V_{\max}} \arcsin(R) \leq t_1 + \frac{1}{V_{\max}} \frac{\pi}{2}$. When t varies from t_1 to T_{out}, the minimum distance $\min_{t \in [t_1, T_{out}]} \|q(t) - A\|^2$ from $q(t)$ to the obstacle can be lower bounded by

$$1 + \min_{t \in [t_1, T_{out}]} f(t)$$

where $f(t) = (1+r)^2 e^{-2t} - (1+r)\frac{2e^{-t}}{1+r} \cos((t-t_1)V_{\max})$. By construction, T_{out} provides a rotation which guarantees that $q(T_{out})$ reaches (OT_1). Then, one must have $f(T_{out}) \geq f(t_2)$. Therefore, f reaches its minimum in the open interval $]t_1, T_{out}[$. The unique minimum t_{min} satisfies $\dot{f}(t_{min}) = 0$, i.e.

$$\begin{aligned}&(1+r)e^{-t_{min}} = \\ &\qquad \cos((t_{min} - t_1)V_{\max}) + \sin((t_{min} - t_1)V_{\max})V_{\max}\end{aligned}$$

After several lines, one finally derives

$$\min_{t \in [t_1, T_{out}]} f(t) = (1 + V_{\max}^2) \sin^2((t_{min} - t_1)V_{\max})$$

Now, one can choose to set

$$V_{\max} \geq \sqrt{\frac{-1}{2} + \sqrt{\frac{1}{2} + \frac{\pi^2 R^2}{2\log^2(\frac{1+r}{1+R})}}}$$

By definition, $r > R$, and thus, $0 < \log(\frac{1+r}{1+R})V_{\max}$. From here, we can consider two exclusive situations. Either $\log(\frac{1+r}{1+R})V_{\max} > \pi/2$ (case 1), or $\log(\frac{1+r}{1+R})V_{\max} \leq \pi/2$ (case 2). In the first case, the total rotation over the time interval $[t_1,t_2]$ guarantees that the trajectory reaches (OT_1). The trajectory does not enter the circle. In the second case, we proceed as follows. By construction of t_1 and t_2, $t_{min} \geq t_2$. By equation (14), $t_{min} - t_1 \geq \log(\frac{1+r}{1+R})$. A lower bound for $f(t)$ is thus given by

$$\min_{t \in [t_1, T_{out}]} f(t) \geq 2(V_{\max}^2 + 1) \sin^2(\log(\frac{1+r}{1+R})V_{\max})$$

Using that $x \geq \sin(x) \geq \frac{2}{\pi}x$ for $x \in [0, \frac{\pi}{2}]$, we derive the following lower bound for $f(t)$ on $[t_1, t_2]$

$$\min_{t\in[t_1,T_{out}]} f(t) \geq R^2$$

This contradicts the existence of an intersecting point q_2. Both cases are inconsistent with the original intersection assumption. This concludes the proof. The proposed condition (12) guarantees obstacle avoidance. ■

We are now interested in trajectories originating in the line sector (OA, OT_2). We remark from (11) that the argument is always decreasing along these, and that the norm is also always decreasing. Let us consider a given point in the line

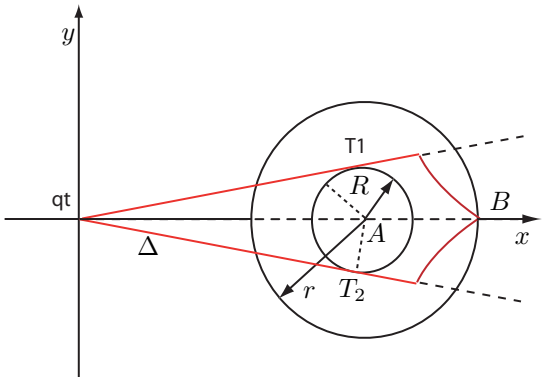

Fig. 10. Invariant set and limit trajectories.

sector (OA, OT_2), outside Δ and look for the trajectory originating at this point.

Definition 2: We note $\mathcal{S}$ the symmetry with respect to the horizontal axis (Ox).

Proposition 3: Consider a point M strictly below the x axis and outside Δ. Consider $\mathcal{S}(M)$. The trajectory $\mathcal{T}(M)$ originating in M is symmetrical to the trajectory originating in $\mathcal{S}(M)$. We have

$$\mathcal{S}(\mathcal{T}(M)) = \mathcal{T}(\mathcal{S}(M))$$

Proof: The symmetry $\mathcal{S}$ has an analytical expression $\mathcal{S}\begin{pmatrix} x \\ y \end{pmatrix} = \begin{pmatrix} x \\ -y \end{pmatrix}$. The differential equation (9) shows a difference in ε when one crosses the x axis. For all $t \geq 0$, we note $\mathcal{T}_t(M)$ the point of the trajectory initiated in M after time t. For all $t \geq 0$, we have

$$\begin{aligned}
&\mathcal{S}(\mathcal{T}_t(\mathcal{S}(M))) \\
=&\mathcal{S}\left(\int_0^t \begin{pmatrix} -1 & \varepsilon_M(t)V_{\max} \\ -\varepsilon_M(t)V_{\max} & -1 \end{pmatrix} \begin{pmatrix} x_M \\ -y_M \end{pmatrix}\right) \\
=&\mathcal{T}_t(M)
\end{aligned}$$

Let us now consider a trajectory starting from a point below the x axis. Using the result above and (2), we can deduce that the trajectory does not intersect the boundary of Δ. The obstacle is thus avoided. ■

Theorem 1: Consider equation (9). Provided that $V_{\max}$ satisfies (12), and that the initial condition is chosen inside Δ, the trajectory avoids the obstacle and exponentially reaches the target 0.

IV. Conclusion

As a conclusion, we could like to stress once again the importance of combining *in practical experiments* the two presented control strategy. We believe that with short-range detection devices, the modified gyroscopic forces approach will adequately complement the trajectory optimisation strategy. Mathematical study of this combination (in terms of performance and convergence analysis), as well as actual implementation are the next goals of our research program.

Acknowledgement: We thank Gaël Desilles for providing experimental facilities, Alain Martin for designing the hybrid GPS/odometer/gyroscope localization system, Nicolas Douziech for implementing the optimal trajectory generation software and helping during the numerous experiments, and Pierre Finance and Johann Forgeard for designing, machine tooling, and interfacing numerous onboard sensors.

References

[1] R. Bhattacharya. OPTRAGEN a Matlab toolbox for optimal trajectory generation. User's manual, Aerospace Engineering Department, Texas A& M University, 2006.

[2] D. E. Chang and J. E. Marsden. Gyroscopic forces and collision avoidance with convex obstacles. *Nonlinear Dynamics and Control*, 295:145–160, 2003.

[3] D. E. Chang, S. Shadden, J. E. Marsden, and R. Olfati-Saber. Collision avoidance for multiple agent systems. In *Proc. of the 42nd IEEE Conf. on Decision and Control*, 2003.

[4] M. Fliess, J. Lévine, P. Martin, and P. Rouchon. A Lie-Bäcklund approach to equivalence and flatness of nonlinear systems. *IEEE Trans. Automat. Control*, 44:922–937, 1999.

[5] C. Guarino Lo Bianco, A. Piazzi, and Romano M. Smooth motion generation for unicycle mobile robots via dynamic path inversion. *IEEE Tr. on robotics*, 20(5):884–892, 2004.

[6] M. B. Milam. *Real-time optimal trajectory generation for constrained systems*. PhD thesis, California Institute of Technology, 2003.

[7] M. B. Milam, K. Mushambi, and R. M. Murray. A new computational approach to real-time trajectory generation for constrained mechanical systems. In *IEEE Conference on Decision and Control*, 2000.

[8] R. M. Murray, J. Hauser, A. Jadbabaie, M. B. Milam, N. Petit, W. B. Dunbar, and R. Franz. Online control customization via optimization-based control. In T. Samad and G. Balas, editors, *Software-Enabled Control, Information technology for dynamical systems*, pages 149–174. Wiley-Interscience, 2003.

[9] Department of Defense. Network centric warfare. Technical report, Report to Congress, 2001.

[10] R. Rao, V. Kumar, and C. Taylor. Visual servoing of a UGV from a UAV using differential flatness. In *Proc. of the 2003 IEEE/RSJ Int. Conference on Intelligent Robots and Systems*, 2003.